# Hydrodynamic phonon drift and second sound in a (20,20) single-wall carbon nanotube

Sangyeop Lee and Lucas Lindsay

Phys. Rev. B **95**, 184304 — Published 18 May 2017

DOI: 10.1103/PhysRevB.95.184304

# Hydrodynamic phonon drift and second sound in a (20,20) single-wall carbon nanotube

Sangyeop Lee[1,2*] and Lucas Lindsay[3]

[1] Department of Mechanical Engineering and Materials Science,
University of Pittsburgh, Pittsburgh PA 15261

[2] Department of Physics and Astronomy,
University of Pittsburgh, Pittsburgh PA 15261

[3] Oak Ridge National Laboratory,
P.O. Box 2008, Oak Ridge, TN 37831

[*] sylee@pitt.edu

**ABSTRACT**

Two hydrodynamic features of phonon transport, phonon drift and second sound, in a (20,20) single wall carbon nanotube (SWCNT) are discussed using lattice dynamics calculations employing an optimized Tersoff potential for atomic interactions. We formally derive a formula for the contribution of drift motion of phonons to total heat flux at steady state. It is found that the drift motion of phonons carry more than 70% and 90% of heat at 300 K and 100 K, respectively, indicating that phonon flow can be reasonably approximated as hydrodynamic if the SWCNT is long enough to avoid ballistic phonon transport. The dispersion relation of second sound is derived from the Peierls-Boltzmann transport equation with Callaway's scattering model and quantifies the speed of second sound and its relaxation. The speed of second sound is around 4000 m/s in a (20,20) SWCNT and the second sound can propagate more than 10 μm in an isotopically pure (20,20) SWCNT for frequency around 1 GHz at 100 K.

## I. INTRODUCTION

Single wall carbon nanotubes (SWCNTs) have received significant attention due to their unique electrical, mechanical and thermal properties[1,2]. In particular, thermal conductivities of SWCNTs are remarkably high[3–5], making them well suited for thermal management applications including electronics packaging and thermal interface materials. Like other carbon-based materials, the high thermal conductivity of SWCNTs can be attributed to the small mass of carbon and stiff covalent bonding, resulting in high Debye temperatures. High Debye temperature accompanies large group velocities of heat-carrying acoustic phonons and generally weak Umklapp three-phonon scattering (hereafter U-scattering) at room temperature, both of which contribute to high thermal conductivity. Another characteristic of materials with a high Debye temperature is long mean free path of phonons due to weak U-scattering. As the typical length of SWCNTs (few micrometers) from experiment[5,6] is comparable to the U-scattering limited mean free paths, phonon-boundary scattering is important and thermal transport has been often discussed as being between ballistic and diffusive regimes for typical SWCNTs[7–9].

Like these transport regimes, hydrodynamic transport has also been extensively studied as another regime of phonon transport in various systems[10–13]. These three regimes (ballistic, diffusive, and hydrodynamic) arise from the dominance of different types of phonon scattering mechanisms. The ballistic regime has very little internal phonon scattering and diffuse phonon-boundary scattering is the dominant resistance. The diffusive regime, on the other hand, has strong U-scattering which destroys overall crystal momentum and boundary scattering is typically weak compared to it. The hydrodynamic regime occurs when normal three-phonon scattering (hereafter N-scattering) is much stronger than U-scattering and boundary scattering. Unlike U-scattering and diffuse boundary scattering, N-scattering always conserves the overall phonon crystal momentum[14], similar to intermolecular scattering in fluid flow. Phonons in this hydrodynamic regime exchange momentum through N-scattering until all phonon modes have the same drift velocity, just like molecules in a small fluid element flow together.

Among many hydrodynamic transport phenomena, phonon Poiseuille flow and second sound have been observed in three-dimensional bulk materials but at very low temperature and only for a narrow temperature range: 0.5 K in solid He for Poiseuille flow and 15 K in NaF for second sound[11,12]. More recently, however, two theoretical studies based on first principles calculations have shown that hydrodynamic phonon transport may be observed in graphene at

significantly higher temperature and over a broader range of temperature[15,16]. According to these studies[15,16], the hydrodynamic phenomena may be clearly observed in graphene even at 100 K. This significant hydrodynamic phonon transport is associated with flexural acoustic phonon modes of graphene. As graphene and SWCNTs are similar in terms of lattice dynamics, hydrodynamic phonon transport may also be significant in SWCNTs, which exhibit two flexural phonon branches and very strong N-scattering[17].

In this paper, we discuss the drift motion of phonons and second sound in a (20,20) SWCNT. Phonon Poiseuille flow is excluded from our discussion as it requires at least a two-dimensional space; transport in SWCNTs is limited to one dimension. We quantitatively demonstrate how much of the actual phonon flow resembles hydrodynamic drift motion. We also show the dispersion relation of second sound and discuss the propagation and relaxation of second sound in (20,20) SWCNTs. Second sound in SWCNTs was previously studied using classical molecular dynamics calculations; however, simulations were limited to very small time and space scales, few picoseconds and around ten nanometers[18,19].

## II. PHONON DRIFT MOTION AND THERMAL TRANSPORT

When a temperature gradient exists in solid materials, phonons exhibit an asymmetric distribution in reciprocal space, causing a net flux of phonon flow. The asymmetric non-equilibrium distribution ( $f_{\mathbf{q}s}^{\mathrm{nonEQ}}$ ) can be expressed with a small deviation ( $u$ ) from the stationary Bose-Einstein distribution:

$$f_{\mathbf{q}s}^{\mathrm{nonEQ}} = \frac{1}{\exp\left(\frac{\hbar\omega_{\mathbf{q}s} - q_\alpha u_\alpha}{k_B T_0}\right) - 1} \tag{1}$$

where $\alpha$ is the temperature gradient direction, $T_0$ is the equilibrium temperature and $\omega_{\mathbf{q}s}$ is phonon frequency for wavevector **q** and polarization *s*. Assuming the deviation term ( $q_\alpha u_\alpha$ ) where $q_\alpha$ is a wavevector along the direction $\alpha$ is much smaller than the phonon energy ( $\hbar\omega_{\mathbf{q}s}$ ), the asymmetric distribution can be linearized as:

$$f_{\mathbf{q}s}^{\mathrm{nonEQ}} \cong f_{\mathbf{q}s}^{0} + \frac{\hbar}{k_B T_0} f_{\mathbf{q}s}^{0}\left(f_{\mathbf{q}s}^{0} + 1\right) q_\alpha u_\alpha \tag{2}$$

where $f_{\mathbf{q}s}^{0}$ is the stationary Bose-Einstein distribution. The second term in the right-hand side represents the asymmetric behavior of the distribution and results in a net phonon flux. In general, the deviation ( $u$ ) depends on wavevector and polarization of a phonon mode. In the hydrodynamic phonon transport regime, however, this deviation is constant regardless of wavevector and polarization indicating that phonons exhibit a collective motion with the same drift velocity represented by $u_\alpha$. The Bose-Einstein distribution with a constant displacement is called the *displaced* (or *drifted*) Bose-Einstein distribution. In the ideal hydrodynamic regime where N-scattering is the only mechanism for phonon scattering, phonons exchange momentum until all phonon modes exhibit the same drift velocity, while preserving the overall crystal momentum. Thus, the displaced Bose-Einstein distribution is an equilibrium state when N-scattering is the only available phonon scattering mechanism.

Although SWCNTs exhibit strong N-scattering, the actual phonon transport cannot exhibit the ideal hydrodynamic regime due to non-negligible U-scattering and defect scattering (hereafter R-scattering refers to combined U-scattering and defect scattering) which do not conserve overall crystal momentum. Thus, the actual phonon distribution in SWCNTs is deviated from the displaced Bose-Einstein distribution. Therefore, it is necessary to quantify how much of

the actual phonon flow is close to the ideal hydrodynamic regime. A recent study by Cepelloti et al.[16] assesses the similarity between the actual phonon distribution and the displaced Bose-Einstein distribution by calculating the drift component in the actual phonon distribution. Here, we quantify the similarity between actual phonon flow in a (20,20) SWCNT and the ideal hydrodynamic drift flow of phonons. We formally derive the contribution of this displaced distribution component to the total heat flux based on previous work by Krumhansl[20] as summarized below.

The steady-state Peierls-Boltzmann transport equation (PBE) is:

$$\mathbf{v}_{\mathbf{q}s} \cdot \nabla f_{\mathbf{q}s} = \left( \frac{\partial f_{\mathbf{q}s}}{\partial t} \right)_{\mathrm{C}} \tag{3}$$

where $\left(\partial f_{\mathbf{q}s}/\partial t\right)_{\mathrm{C}}$ is the rate of change of the phonon distribution due to scattering and $\mathbf{v}_{\mathbf{q}s}$ is the phonon velocity. The distribution, $f_{\mathbf{q}s}$, in Eq. (3) and hereafter refers to the non-equilibrium distribution, $f_{\mathbf{q}s}^{\mathrm{nonEQ}}$. Assuming only a small deviation from the stationary Bose-Einstein distribution, the scattering term can be linearized as:

$$\left( \frac{\partial f_{\mathbf{q}s}}{\partial t} \right)_{\mathrm{C}} = \sum_{\mathbf{q}'s'} G_{\mathbf{q}s,\mathbf{q}'s'} f_{\mathbf{q}'s'}^{\mathrm{d}} \tag{4}$$

where $f_{\mathbf{q}s}^{\mathrm{d}}$ is the deviation from equilibrium, defined as $f_{\mathbf{q}s}^{\mathrm{d}} = f_{\mathbf{q}s} - f_{\mathbf{q}s}^{0}$. The $G_{\mathbf{q}s,\mathbf{q}'s'}$ is a scattering matrix element. It would be useful if the eigenstates of Eq. (3) are orthogonal. Then, the total distribution function can be projected onto the specific eigenstate that represents hydrodynamic drift motion of phonons in order to quantify the significance of the hydrodynamic regime. For this purpose, we multiply a factor, $2\sinh(X_{\mathbf{q}s}/2)$, on the both sides of Eq. (3). Here, $X_{\mathbf{q}s}$ is $\hbar\omega_{\mathbf{q}s}/k_B T_0$. Then, the PBE becomes

$$\left( 2\sinh\frac{1}{2}X_{\mathbf{q}s} \right) \mathbf{v}_{\mathbf{q}s} \cdot \nabla f_{\mathbf{q}s} = \sum_{\mathbf{q}'s'} G^{*}_{\mathbf{q}s,\mathbf{q}'s'} f^{\mathrm{d}*}_{\mathbf{q}'s'} \tag{5}$$

where $f^{\mathrm{d}*}_{\mathbf{q}'s'}$ is $\left( 2\sinh\frac{1}{2}X_{\mathbf{q}'s'} \right) f^{\mathrm{d}}_{\mathbf{q}'s'}$ and the scattering matrix, $\mathbf{G}^{*}$, is

$$G^{*}_{\mathbf{q}s,\mathbf{q}'s'} = \left( \frac{2\sinh\frac{1}{2}X_{\mathbf{q}s}}{2\sinh\frac{1}{2}X_{\mathbf{q}'s'}} \right) G_{\mathbf{q}s,\mathbf{q}'s'} \tag{6}$$

Note that the scattering matrix, $\mathbf{G}^*$, is symmetric.

Since the scattering matrix, $\mathbf{G}^*$, is symmetric, the solution of PBE ( $f^{\mathrm{d}*}$ ) can be expressed as a linear combination of orthogonal eigenvectors of $\mathbf{G}^*$. Assuming that N-scattering is much stronger than R-scattering, the scattering matrix, $\mathbf{G}^*$, can be approximated to an N-scattering matrix, $\mathbf{N}^*$. There are two already known eigenvectors of $\mathbf{N}^*$, $|0\rangle$ and $|1_\alpha\rangle$, representing stationary and displaced Bose-Einstein distributions, respectively. The eigenvalues of these two eigenvectors are zero, indicating that these eigenvectors describe equilibrium states under N-scattering. These eigenvectors are:

$$|0\rangle = X_{\mathbf{q}s}\left(2\sinh\frac{1}{2}X_{\mathbf{q}s}\right)^{-1} \tag{7a}$$

$$|1_\alpha\rangle = \frac{q_\alpha}{k_B T}\left(2\sinh\frac{1}{2}X_{\mathbf{q}s}\right)^{-1} \tag{7b}$$

The solution of this PBE can be expressed as a linear combination of orthogonal eigenvectors:

$$f^{\mathrm{d}*} = T'|0\rangle + u_\alpha|1_\alpha\rangle + a_2|2\rangle + \ldots \tag{8}$$

where $T'$ is a local temperature deviation from a global equilibrium temperature ($T_0$), defined as $T'(\mathbf{x},t) = \left(T(\mathbf{x},t) - T_0\right)/T_0$. The eigenvector, $|2\rangle$, and its coefficient, $a_2$, are not known here. The displacement, $u_\alpha$, can be calculated using the orthogonality of the eigenvectors:

$$u_\alpha = \frac{\langle 1_\alpha | f^{\mathrm{d}*}\rangle}{\langle 1_\alpha | 1_\alpha\rangle} \tag{9}$$

The total heat flux can be expressed with contribution from each eigenstate:

$$Q = Q_{|1_\alpha\rangle} + Q_{|2\rangle} + \ldots = \sum_{\mathbf{q}s}\hbar\omega_{\mathbf{q}s}v_{\mathbf{q}s,\alpha}f^{\mathrm{d}}_{\mathbf{q}s,|1_\alpha\rangle} + \sum_{\mathbf{q}s}\hbar\omega_{\mathbf{q}s}v_{\mathbf{q}s,\alpha}f^{\mathrm{d}}_{\mathbf{q}s,|2\rangle} + \ldots \tag{10}$$

where $f^{\mathrm{d}}_{\mathbf{q}s,|1_\alpha\rangle} = \left(2\sinh\frac{1}{2}X_{\mathbf{q}s}\right)^{-1} u_\alpha|1_\alpha\rangle$. We define the contribution from a displacement component to the total heat flux as:

$$\gamma_{|1_\alpha\rangle} = \frac{Q_{|1_\alpha\rangle}}{Q} \tag{11}$$

If the contribution, $\gamma_{|1_\alpha\rangle}$, is close to unity, the total heat flux is mostly due to the displaced eigenstate and heat flow is hydrodynamic. Thus, calculation of this contribution, $\gamma_{|1_\alpha\rangle}$, can quantitatively demonstrate how much of the actual phonon flow resembles an ideal hydrodynamic flow.

The contribution of the displaced distribution component to the total heat flux in a (20,20) SWCNT was calculated using Eq. (11) and shown in Fig. 1. To this end, the non-equilibrium mode distributions, $f^{\mathrm{d}}_{\mathbf{q}s}$, were calculated by solving the PBE described by Eqns. 6-9 in Ref. 7 and using an iterative method[21]. The three-phonon scattering matrix elements (Eq. 2 of Ref. 7) and phonon dispersion required for building these distributions were determined from harmonic and third-order anharmonic force constants derived from numerical differentiation of the optimized Tersoff potential[22]. The (20,20) SWCNT was allowed to fully relax, giving a nearest neighbor C-C distance of 1.440 Å around the circumference of the SWCNT with a slight contraction of 0.05% for bonds along the axis. We note that sum rules dictated by translational and rotational invariance conditions are fully satisfied by this potential[7,23–26], giving two linear (longitudinal and torsional) and two degenerate quadratic (flexural) acoustic branches characteristic of SWCNTs. We note that the optimized Tersoff potential gives a reasonably accurate description of the phonon dispersion[22] and thermal conductivity of graphene[27], and was applied to examine thermal transport of a wide range of SWCNTs previously[17]. We include phonon scattering by mass variation from $^{13}$C isotopes with the naturally occurring isotope content (1.1%)[28]. A homogenous phonon-boundary scattering rate defined as $2|v_{\mathbf{q}s,\alpha}|/L$ is also included assuming a sample size ($L$) of 10 μm.

An issue with calculating the heat flux contribution from the drift component, $\gamma_{|1_\alpha\rangle}$, is the inner product, $\langle 1_\alpha|1_\alpha\rangle$, in Eq. (9) diverges if an acoustic branch has quadratic dispersion in the long-wavelength limit in one-dimensional reciprocal space, as occurs for purely harmonic SWCNTs. This is because the integrand of $\langle 1_\alpha|1_\alpha\rangle$, $q^2\left(2\sinh\frac{1}{2}X_q\right)^{-2}$, diverges. However, this problem is avoided as the long wavelength dispersion of flexural acoustic phonon branches are renormalized by anharmonic interactions. For graphene, similar to large diameter SWCNTs in terms of lattice dynamics, it was reported that the phonon renormalization effect is strong for

wavevectors smaller than the cut-off wavevector, $q_c$=0.14 Å$^{-1}$ at 100 K[29]. To the best of our knowledge a cut-off wavevector of SWCNTs has not been reported yet. Instead, we calculated the displacement defined in Eq. (9) using various values for cut-off wavevector ranging from 0.01 Å$^{-1}$ to 0.1 Å$^{-1}$. The difference in the displacement values is not larger than 5 %.

Fig. 1 shows that the majority of heat in a (20,20) SWCNT from 50 to 300 K is carried by the hydrodynamic drift motion of phonons. Below 100 K, more than 90% of the total heat flux is due to this drift and the phonon flow can be approximated as nearly ideal hydrodynamic flow. As temperature is decreased to 50 K, the contribution of the displaced component to the total heat flux saturates around 95%. This can be associated with the phonon scattering by isotope and boundary. As temperature increases, the drift component contribution decreases due to increasing U-scattering. However, more than 70% of heat is still carried by hydrodynamic phonon drift at 300 K. This indicates that the actual phonon flow in a (20,20) SWCNT can be approximated as hydrodynamic for temperatures below 300 K. Even at very high temperatures hydrodynamic flow provides ~50% to the total heat flux.

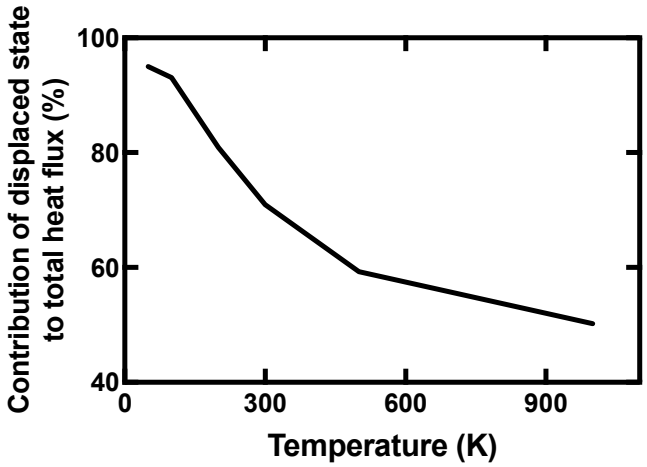


Fig. 1. Contribution of displaced distribution component to the total heat flux in a 10 μm long (20,20) SWCNT with naturally occurring $^{13}$C isotope content (1.1 %).

## III. DISPERSION RELATION OF SECOND SOUND

### A. Second Sound for Ideal Hydrodynamic Regime ($1/\tau_R \to 0$ and $1/\tau_N \to \infty$)

The ideal hydrodynamic regime is assumed when R-scattering is weak ($1/\tau_R \to 0$) and N-scattering is extremely strong ($1/\tau_N \to \infty$). The momentum and energy balance equations from the PBE are:

$$\frac{\partial P_\alpha}{\partial t} + \frac{\partial \theta_{\alpha\beta}}{\partial x_\alpha} = 0 \tag{12a}$$

$$\frac{\partial \varepsilon}{\partial t} + \frac{\partial Q_\alpha}{\partial x_\alpha} = 0 \tag{12b}$$

where $P_\alpha = \sum_{\mathbf{q}s} q_\alpha f_{\mathbf{q}s}$ and $\varepsilon = \sum_{\mathbf{q}s} \hbar\omega_{\mathbf{q}s} f_{\mathbf{q}s}$ are momentum and energy densities, and $\theta_{\alpha\beta} = \sum_{\mathbf{q}s} q_\alpha v_{\mathbf{q}s\beta} f_{\mathbf{q}s}$ and $Q_\alpha = \sum_{\mathbf{q}s} \hbar\omega_{\mathbf{q}s} v_{\mathbf{q}s\alpha} f_{\mathbf{q}s}$ are momentum and energy fluxes. The right-hand side of the momentum balance equation is zero because the total crystal momentum is always conserved in the ideal case where N-scattering is the only scattering mechanism. The right-hand side of the energy balance equation is also zero because the total energy is always conserved upon scattering.

For the ideal case where $1/\tau_{\mathrm{R}} \to 0$ and $1/\tau_{\mathrm{N}} \to \infty$, the solution of the PBE is:

$$f^{\mathrm{d}} = \left(2\sinh\frac{1}{2}X\right)^{-1}\left(T'(\mathbf{x},t)\left|0\right\rangle + u_\alpha(\mathbf{x},t)\left|1_\alpha\right\rangle\right) \tag{13}$$

Substituting this into Eq. (12) gives:

$$\left\langle 1_\alpha \middle| 1_\alpha \right\rangle \frac{\partial u_\alpha}{\partial t} + \left\langle 0 \middle| v_\alpha \middle| 1_\alpha \right\rangle \frac{\partial T'}{\partial x_\alpha} = 0 \tag{14a}$$

$$\left\langle 0 \middle| 0 \right\rangle \frac{\partial T'}{\partial t} + \left\langle 0 \middle| v_\alpha \middle| 1_\alpha \right\rangle \frac{\partial u_\alpha}{\partial x_\alpha} = 0 \tag{14b}$$

Combined, these equations give an expression for the speed of second sound:

$$v_{\mathrm{II},\alpha}^2 = \frac{\left\langle 0 \middle| v_\alpha \middle| 1_\alpha \right\rangle^2}{\left\langle 0 \middle| 0 \right\rangle \left\langle 1_\alpha \middle| 1_\alpha \right\rangle} \tag{15}$$

We note that a slightly different expression for the speed of second sound was derived using the heat flux and energy balance equations[16,30], while Eq. (15) is from the momentum and energy balance equations. The heat flux balance equation can be derived from the PBE by multiplying energy and group velocity and integrating the equation over the first Brillouin zone

and summing over phonon branches. The heat flux balance equation with the solution of the PBE in Eq. (13) is:

$$\langle 0|v_\alpha|1_\alpha\rangle \frac{\partial u_\alpha}{\partial t} + \langle 0|v_\alpha^2|0\rangle \frac{\partial T'}{\partial x_\alpha} = 0 \tag{16}$$

The right-hand side is zero, because it was assumed that heat flux is conserved upon scattering when N-scattering is the only scattering mechanism[16]. The resulting expression for the speed of second sound from Eq. (16) and (14b) is:

$$v_{\mathrm{II},\alpha}^2 = \frac{\langle 0|v_\alpha^2|0\rangle}{\langle 0|0\rangle} \tag{17}$$

In Fig. 2, we compare the speed of second sound of (20,20) SWCNTs from the two different expressions in Eq. (15) and (17). These expressions give remarkably different values for the speed of second sound: ~4000 m/s from Eq. (15) and ~6000-8000 m/s from Eq. (17) depending on temperature. We attribute this difference to the assumption that heat flux is conserved upon scattering. The heat flux balance equation (Eq. 16) assumes that total heat flux is always conserved when N-scattering is the only scattering mechanism. However, this assumption is valid only when phonon group velocities are constant and the dispersion is isotropic as in the Debye model. Under these conditions N-scattering leads to the conservation of heat flux ( $\mathbf{v}\omega_1 + \mathbf{v}\omega_2 = \mathbf{v}\omega_3$ ). However, when the phonon dispersion is non-linear and many phonon branches have different group velocities as in SWCNTs and other systems, the conservation of energy and momentum does not necessarily lead to the conservation of heat flux, namely $\mathbf{v}_1\omega_1 + \mathbf{v}_2\omega_2 \neq \mathbf{v}_3\omega_3$ where $\mathbf{v}_1 \neq \mathbf{v}_2 \neq \mathbf{v}_3$. Therefore, the total heat flux is not conserved upon N-scattering in SWCNTs even if N-scattering is the only scattering mechanism. For this reason, we believe that the speed of second sound should be derived from the momentum balance equation rather than the heat flux balance equation, when phonon group velocities are not constant. It is noteworthy that Eq. (15) and (17) are identical if the Debye model is assumed. Another type of second sound, called driftless second sound, was also mathematically derived from a heat flux balance equation with a damping term for the heat flux[30]. We exclude this driftless second sound in our discussion as it has not been experimentally confirmed to the best of our knowledge and does not require hydrodynamic drift motion of phonons. The driftless second sound is an extraordinary case of the diffusive regime (Fourier's law) when all eigenstates of the distribution function exponentially decay with the same relaxation time[30].

The fact that N-scattering does not conserve heat flux may seem to conflict with the famous Peierl's thought experiment that shows the conservation of heat flux upon N-scattering[14]. However, second sound and Peierl's thought experiment assume different conditions. Second sound involves spatial and temporal variance of the phonon distribution due to a fluctuating temperature field, whereas Peierl's thought experiment assumes the phonon distribution does not vary in time and space[14]. In the Peierl's thought experiment, if N-scattering is the only scattering mechanism, the phonon flow that already has the displaced Bose-Einstein distribution can persist without relaxation even when there is no driving force, i.e., a temperature gradient. In this case, the drift velocity or displacement of the phonon distribution is a constant in space and time. This distribution is unaltered by N-scattering, thus the total heat flux is not changed. However, in the case of second sound, we have a spatially and temporally varying temperature field. Due to this varying temperature field, the distribution of phonons advected from nearby locations differ from the phonon distribution at the current location. This difference in distribution is relaxed by many N-scattering events, establishing local equilibrium. If phonons have different group velocities, N-scattering does not necessarily conserve heat flux during this relaxation process.

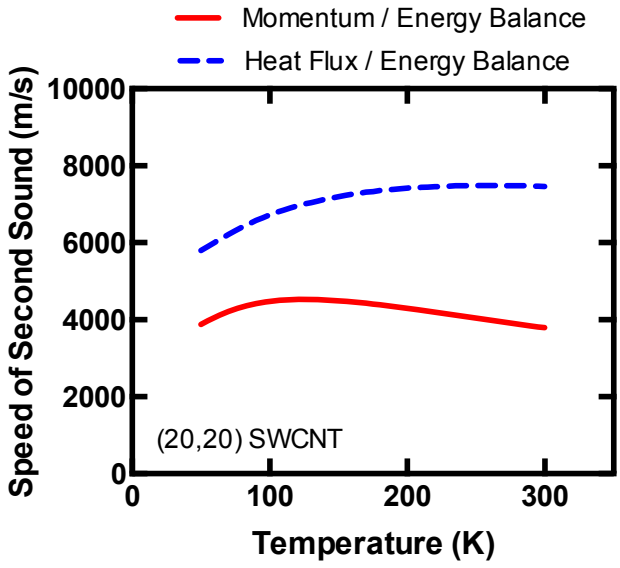


Fig. 2. Comparison of speeds of second sound in a (20,20) SWCNT from momentum/energy balance equations and heat flux/energy balance equations.

The speed of second sound has often been compared to the group velocity of acoustic phonons (speed of first sound), and this comparison has played an important role for the observation of second sound in past experimental studies[11,31]. Here, we compare the propagation speeds of ballistic phonon transport and second sound in a (20,20) SWCNT. We assume that a heat pulse is generated at one end of the SWCNT sample at $t$=0. For ballistic phonon transport, the temperature increase at the opposite end of the sample can be calculated as[15]:

$$\frac{dT}{dt}(t) \sim \sum_{\mathbf{q}s} \hbar\omega_{\mathbf{q}s} \frac{df^0_{\mathbf{q}s}}{dT} \delta\left(L - v_{\mathbf{q}s} t\right) \tag{18}$$

where $L$ is the sample length. The calculated arrival times per sample length for ballistic phonon transport and second sound are shown in Fig. 3. The ballistic phonon transport cases exhibit a very broad curve because the phonon group velocities in SWCNTs vary significantly depending on wavevector and polarization. From Fig. 3, the propagation speed of second sound is slower than that of the ballistic phonon transport peak by a factor of 1.5, similar to the 3D Debye model where the speed of second sound is slower than the speed of acoustic sound by $\sqrt{3}$.

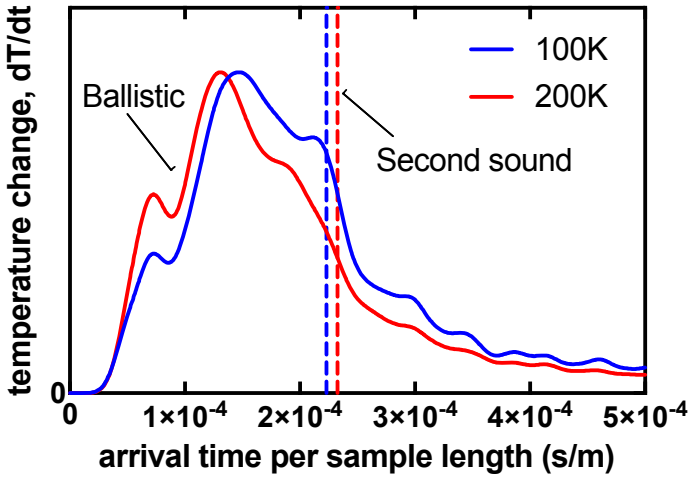


Fig. 3. Comparison of propagation speeds of ballistic phonon transport and second sound at 100 K and 200 K. The temperature change in y-axis is in linear scale. For comparison, the arrival times per sample length of longitudinal and torsional acoustic phonons that propagate ballistically are $4.6\times10^{-5}$ s/m and $6.7\times10^{-5}$ s/m, respectively.

**B. Second Sound for the Actual Case ($1/\tau_R$ and $1/\tau_N$ are finite)**

In the previous case where R-scattering was not considered and N-scattering is very strong, second sound can propagate without relaxation. However, in the actual case where $1/\tau_{\mathrm{R}}$ and $1/\tau_{\mathrm{N}}$ are both finite, these can result in the relaxation of second sound as R-scattering does not conserve the total crystal momentum and N-scattering gives viscous dissipation. A dispersion relation of second sound including these relaxation mechanisms can be derived based on Callaway's scattering model[32]. A similar derivation was reported elsewhere assuming linear phonon dispersion[13]. Here we assume a general case where phonon dispersion is non-linear and many phonon branches are involved in thermal transport.

The PBE with Callaway's scattering model is:

$$\frac{\partial f_{\mathbf{q}s}}{\partial t}+\mathbf{v}_{\mathbf{q}s}\cdot\nabla f_{\mathbf{q}s}=-\frac{f_{\mathbf{q}s}-f_{\mathbf{q}s}^{\mathrm{disp}}}{\tau_{\mathrm{N}}}-\frac{f_{\mathbf{q}s}-f_{\mathbf{q}s}^{0}}{\tau_{\mathrm{R}}} \tag{19}$$

where $f_{\mathbf{q}s}^{0}$ is the stationary Bose-Einstein distribution with a local equilibrium temperature, $T_0+\delta T\left(\mathbf{x},t\right)$:

$$f_{\mathbf{q}s}^{0}=\frac{1}{\exp\left(\dfrac{\hbar\omega_{\mathbf{q}s}}{k_B\left(T_0+\delta T\right)}\right)-1} \tag{20}$$

$f_{\mathbf{q}s}^{\mathrm{disp}}$ represents the displaced Bose-Einstein distribution. Eq. (19) can be simplified by replacing $f_{\mathbf{q}s}$ on the left-hand side by $f_{\mathbf{q}s}^{\mathrm{disp}}$:

$$\frac{\partial f_{\mathbf{q}s}^{\mathrm{disp}}}{\partial t}+\mathbf{v}_{\mathbf{q}s}\cdot\nabla f_{\mathbf{q}s}^{\mathrm{disp}}=-\frac{f_{\mathbf{q}s}-f_{\mathbf{q}s}^{\mathrm{disp}}}{\tau_{\mathrm{N}}}-\frac{f_{\mathbf{q}s}-f_{\mathbf{q}s}^{0}}{\tau_{\mathrm{R}}} \tag{21}$$

This simplification corresponds to the Chapman-Enskog expansion to the first order in Knudsen number, which has been used for molecular flow[33]. The Knudsen number in phonon hydrodynamics can be defined as $v_{\mathbf{q}s}\tau_{\mathrm{N}}/L$ where $L$ is a characteristic length of a system. For second sound, $L$ is the wavelength of second sound and making the substitution is well justified when $v\tau_{\mathrm{N}}$ is much smaller than this.

It is straightforward to solve Eq. (21) with the solution being:

$$f^{\mathrm{d}*}=T'\left|0\right\rangle+\left(\frac{\tau_{\mathrm{C}}}{\tau_{\mathrm{N}}}\right)u_\alpha\left|1_\alpha\right\rangle-\tau_{\mathrm{C}}\left(\frac{\partial T'}{\partial t}+v_\alpha\frac{\partial T'}{\partial x_\alpha}\right)\left|0\right\rangle-\tau_{\mathrm{C}}\left(\frac{\partial u_\alpha}{\partial t}+v_\alpha\frac{\partial u_\alpha}{\partial x_\alpha}\right)\left|1_\alpha\right\rangle \tag{22}$$

where $1/\tau_C = 1/\tau_N + 1/\tau_R$. Note that the solution in this case differs from the ideal case. First, the displaced component, $u_\alpha |1_\alpha\rangle$, has an additional coefficient, $\tau_C / \tau_N$, which approaches unity when $\tau_R$ goes to infinity, thus recovering the solution of the ideal case. On the other hand, when $\tau_R$ approaches zero, the coefficient, $\tau_C / \tau_N$, becomes zero, making the displaced component disappear. Second, we have additional third and fourth terms indicating that the phonon distribution at one location is affected by the phonon distribution in its vicinity as represented by the temporal and spatial gradient of displacement and temperature. These terms contribute to a viscous damping effect.

The momentum and energy balance equations can be derived from the PBE. A difference from the ideal case is that we have a momentum destroying term on the right hand-side of the momentum balance equation due to R-scattering:

$$\frac{\partial P_\alpha}{\partial t} + \frac{\partial \theta_{\alpha\beta}}{\partial x_\alpha} = \sum_{\mathbf{q}s} -\mathbf{q}\frac{f_{\mathbf{q}s} - f^0_{\mathbf{q}s}}{\tau_R} \tag{23a}$$

$$\frac{\partial \varepsilon}{\partial t} + \frac{\partial Q_\alpha}{\partial x_\alpha} = 0 \tag{23b}$$

We substitute the solution of the PBE (Eq. (22)) into the above equations and assume that the displacement and temperature fields fluctuate in the form of a plane wave with frequency, $\Omega$, and wavevector, $\mathbf{k}$:

$$u_\alpha(\mathbf{x},t) = u_{\alpha 0} e^{i(\Omega t - \mathbf{k}\cdot\mathbf{x})} \tag{24a}$$

$$T'(\mathbf{x},t) = T'_0 e^{i(\Omega t - \mathbf{k}\cdot\mathbf{x})} \tag{24b}$$

The resulting momentum and energy balance equations are:

$$A_{11}T'_0 + A_{12}u_{\alpha 0} = 0 \tag{25a}$$

$$A_{21}T'_0 + A_{22}u_{\alpha 0} = 0 \tag{25b}$$

where:

$$A_{11} = -2\langle 0|v_\alpha \tau_C|1_\alpha\rangle k_\alpha \Omega - i\langle 0|v_\alpha(1-\tau_C/\tau_R)|1_\alpha\rangle k_\alpha \tag{26a}$$

$$A_{12} = \langle 1_\alpha|\tau_C|1_\alpha\rangle \Omega^2 + \langle 1_\alpha|{v_\alpha}^2\tau_C|1_\alpha\rangle {k_\alpha}^2 + \langle 1_\alpha|\tau_C/(\tau_N\tau_R)|1_\alpha\rangle + i\langle 1_\alpha|\tau_C(1/\tau_N - 1/\tau_R)|1_\alpha\rangle \Omega \tag{26b}$$

$$A_{21} = \langle 0|\tau_C|0\rangle \Omega^2 + \langle 0|{v_\alpha}^2\tau_C|0\rangle {k_\alpha}^2 + i\langle 0|0\rangle \Omega \tag{26c}$$

$$A_{22} = -2\langle 0|v_\alpha \tau_C|1_\alpha\rangle k_\alpha \Omega - i\langle 0|v_\alpha \tau_C/\tau_N|1_\alpha\rangle k_\alpha \tag{26d}$$

For the second sound wave to exist, the determinant of **A** should be zero, giving the dispersion relation of second sound.

We calculated the dispersion relation of second sound (frequency vs. wavevector) satisfying this condition as shown in Fig. 4 for various temperatures. For small wavevector the imaginary component is comparable or larger than the real component giving relaxation of second sound. This is dominated by crystal momentum destroying U-scattering. In this case, the temperature field slowly varies in time and space and the viscous damping by N-scattering is not effective. As the U-scattering does not depend on the wavevector of second sound, the imaginary frequency component does not vary with the wavevector, imposing a lower limit of the wavevector and frequency of second sound. As the second sound wavevector increases, the temperature field varies rapidly in space and the viscous damping by N-scattering becomes stronger. This viscous damping mechanism imposes the upper limit of the wavevector and frequency of second sound. Between these limits, second sound can propagate without significant relaxation. The dispersion relation in Fig. 4 provides the range of second sound frequency that may be observed in (20,20) SWCNTs. The second sound frequency has a wide range from 1 MHz to 100 MHz at 50 K. As temperature increases, the range of second sound frequency increases and becomes narrower since U-scattering rates increase.

(a)

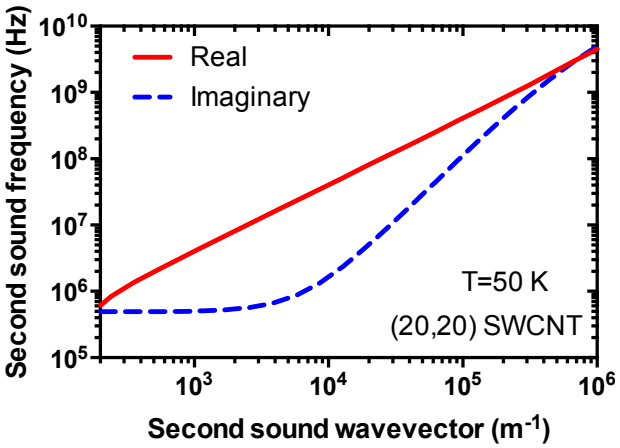


(b)

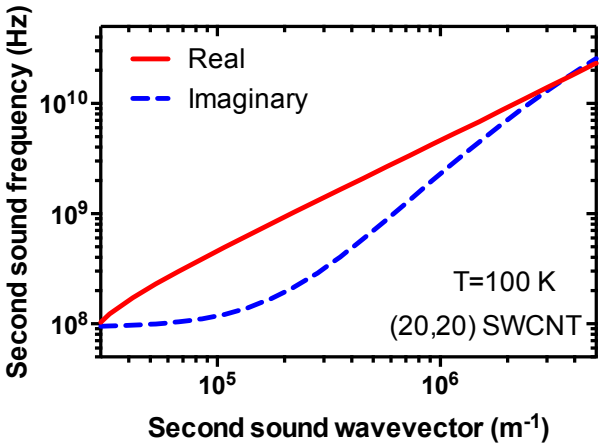


(c)

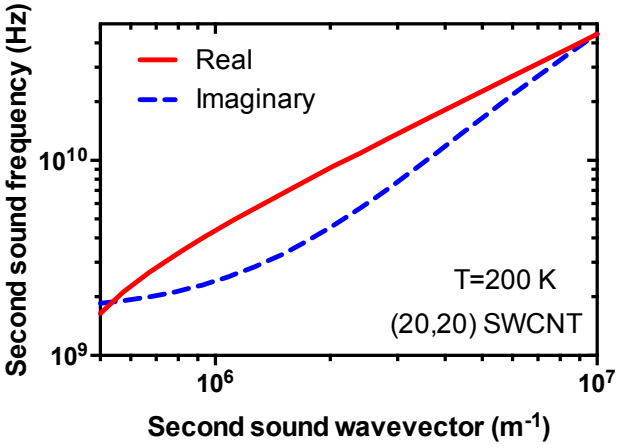


Fig. 4 Dispersion relation of second sound in an isotopically pure (20,20) SWCNT at (a) 50 K, (b) 100 K, and (c) 200 K

In addition to the second sound frequency range, the length of SWCNT samples also should be considered when observing second sound. The sample length should be larger than the wavelength but smaller than the relaxation length of second sound. Here, we define the relaxation length of second sound as $v_{II}\mathrm{Im}(\Omega)$. The wavelength and relaxation length of second sound impose the lower and upper limits, respectively, of the sample length for which this phenomena may be observed. Similar to the second sound frequency, the required length of the sample decreases as temperature increases because U-scattering rates increase. From Fig. 5, a 10 μm long sample would be adequate to observe second sound when the temperature is 100 K.

It would be also interesting to compare SWCNTs with different diameters regarding second sound, though computationally costly. Preliminary calculations for smaller diameter tubes demonstrate that observation of hydrodynamic transport is not as favorable. Further, given the previous results for graphene[15,16] we would expect larger diameter tubes to be more promising to experimentally observe second sound.

(a)

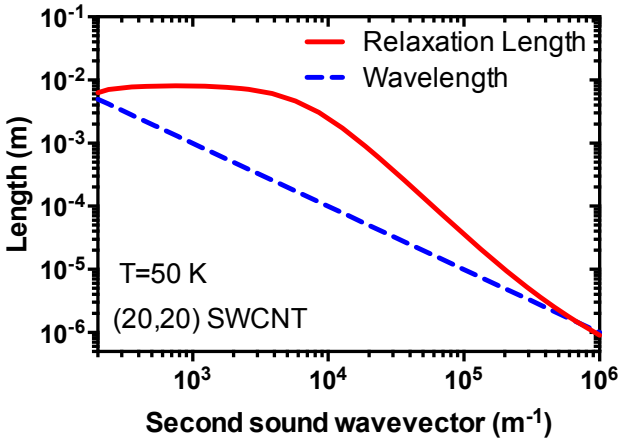


(b)

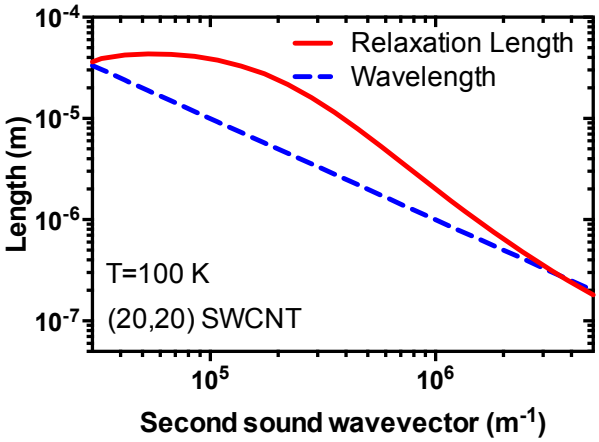


(c)

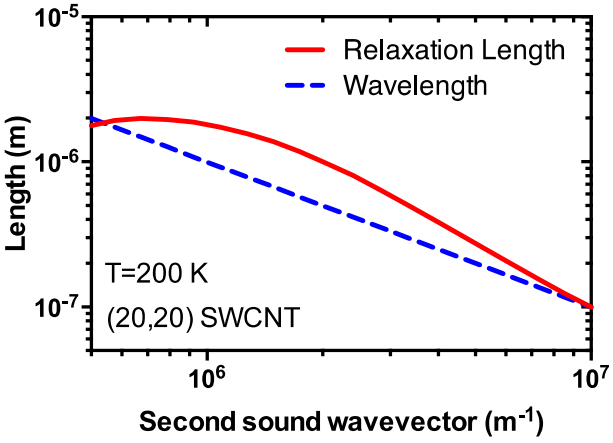


Fig. 5 Relaxation length of second sound in isotopically pure (20,20) SWCNT at (a) 50 K, (b) 100 K, and (c) 200 K

## IV. CONCLUSIONS

We investigated hydrodynamic phonon drift and second sound in a (20,20) SWCNT using lattice dynamics calculations and the Peierls-Boltzmann transport equation (PBE). For hydrodynamic drift motion, the contribution of the drift distribution component to the total heat flux was formally derived and shown to carry 70% of the total heat in a (20,20) SWCNT with naturally occurring isotope content at 300 K. Below 100 K, more than 90% of the total heat is carried by the drift motion of phonons. Propagation and relaxation of second sound was also quantitatively studied. The dispersion relation of second sound was derived from the PBE using the Chapman-Enskog expansion to first order in the phonon Knudsen number. The second sound in a (20,20) SWCNT propagates at a speed of ~ 4000 m/s, slower than the ballistic transport of longitudinal and torsional acoustic phonon modes of which group velocities are 22000 m/s and 15000 m/s, respectively. The second sound dispersion relation shows the relaxation of second sound due to viscous damping from N-scattering as well as direct momentum destroying from R-scattering, providing conditions to observe second sound in (20,20) SWCNTs. It was found that the relaxation of second sound can be minimized when the frequency of second sound is around 1 GHz at 100 K and the second sound can propagate more than 10 μm for these conditions.

## ACKNOWLEDGEMENTS

S.L. acknowledges a support from the Central Research Development Fund of University of Pittsburgh (#9012883). L. L. acknowledges support from the U. S. Department of Energy, Office of Science, Office of Basic Energy Sciences, Materials Sciences and Engineering Division.

## REFERENCES


[1] R.E. Smalley, M.S. Dresselhaus, G. Dresselhaus, and P. Avouris, *Carbon Nanotubes: Synthesis, Structure, Properties, and Applications* (Springer Science & Business Media, 2003).

[2] R.H. Baughman, A.A. Zakhidov, and W.A. de Heer, Science (80-. ). **297**, 787 LP (2002).

[3] J. Hone, M. Whitney, C. Piskoti, and A. Zettl, Phys. Rev. B **59**, R2514 (1999).

[4] S. Berber, Y.-K. Kwon, and D. Tománek, Phys. Rev. Lett. **84**, 4613 (2000).

[5] E. Pop, D. Mann, Q. Wang, K. Goodson, and H. Dai, NANO Lett. **6**, 96 (2006).

[6] C. Yu, L. Shi, Z. Yao, D. Li, and A. Majumdar, NANO Lett. **5**, 1842 (2005).

[7] L. Lindsay, D.A. Broido, and N. Mingo, Phys. Rev. B **80**, 125407 (2009).

[8] J. Shiomi and S. Maruyama, Jpn. J. Appl. Phys. **47**, 2005 (2008).

[9] J. Wang and J.-S. Wang, Appl. Phys. Lett. **88**, 111909 (2006).

[10] R.A. Guyer and J.A. Krumhansl, Phys. Rev. **148**, 778 (1966).

[11] T.F. McNelly, S.J. Rogers, D.J. Channin, R.J. Rollefson, W.M. Goubau, G.E. Schmidt, J.A. Krumhansl, and R.O. Pohl, Phys. Rev. Lett. **24**, 100 (1970).

[12] R.N. Gurzhi, J. Exp. Theor. Phys. **46**, 719 (1964).

[13] H. Beck, P.F. Meier, and A. Thellung, Phys. Status Solidi **24**, 11 (1974).

[14] R.E. Peierls, *Quantum Theory of Solids* (Oxford University Press, 1955).

[15] S. Lee, D. Broido, K. Esfarjani, and G. Chen, Nat. Commun. **6**, 6290 (2015).

[16] A. Cepellotti, G. Fugallo, L. Paulatto, M. Lazzeri, F. Mauri, and N. Marzari, Nat. Commun. **6**, (2015).

[17] L. Lindsay, D.A. Broido, and N. Mingo, Phys. Rev. B **82**, 161402 (2010).

[18] M.A. Osman and D. Srivastava, Phys. Rev. B **72**, 125413 (2005).

[19] J. Shiomi and S. Maruyama, Phys. Rev. B **73**, 205420 (2006).

[20] J.A. Krumhansl, Proc. Phys. Soc. **85**, 921 (1965).

[21] M. Omini and A. Sparavigna, Phys. Rev. B **53**, 9064 (1996).

[22] L. Lindsay and D.A. Broido, Phys. Rev. B **81**, 205441 (2010).

[23] M. Born and K. Huang, *Dynamical Theory of Crystal Lattices* (Clarendon press, 1954).

[24] G. Leibfried and W. Ludwig, Solid State Phys. **12**, 275 (1961).

[25] V.N. Popov, V.E. Van Doren, and M. Balkanski, Phys. Rev. B **61**, 3078 (2000).

[26] G.D. Mahan and S.J. Gun, Phys. Rev. B - Condens. Matter Mater. Phys. **70**, 1 (2004).

[27] L. Lindsay, W. Li, J. Carrete, N. Mingo, D.A. Broido, and T.L. Reinecke, Phys. Rev. B **89**, 155426 (2014).

[28] S. Tamura, Phys. Rev. B **30**, 849 (1984).

[29] R. Roldán, A. Fasolino, K. V Zakharchenko, and M.I. Katsnelson, Phys. Rev. B **83**, 174104 (2011).

[30] R.J. Hardy, Phys. Rev. B **2**, 1193 (1970).

[31] V. Narayanamurti and R.C. Dynes, Phys. Rev. Lett. **28**, 1461 (1972).

[32] J. Callaway, Phys. Rev. **113**, 1046 (1959).

[33] W.G. Vincenti and C.H. Kruger, *Introduction to Physical Gas Dynamics* (Wiley, New York, 1965).